Transition to Landau levels in graphene quantum dots

F. Libisch,[1,*] S. Rotter,[1] J. Güttinger,[2] C. Stampfer,[2,3] and J. Burgdörfer[1]
[1]*Institute for Theoretical Physics, Vienna University of Technology, Wiedner Hauptstraße 8-10/136, A-1040 Vienna, Austria, EU*
[2]*Solid State Physics Laboratory, ETH Zurich, 8093 Zurich, Switzerland*
[3]*JARA-FIT and II. Institute of Physics, RWTH Aachen, 52074 Aachen, Germany, EU*
(Received 4 March 2010; revised manuscript received 19 May 2010; published 8 June 2010)

We investigate the electronic eigenstates of graphene quantum dots of realistic size (up to 80 nm diameter) in the presence of a perpendicular magnetic field B. Numerical tight-binding calculations and Coulomb-blockade measurements performed near the Dirac point exhibit the transition from the linear density of states at $B=0$ to the Landau-level regime at high fields. Details of this transition sensitively depend on the underlying graphene lattice structure, bulk defects, and localization effects at the edges. Key to the understanding of the parametric evolution of the levels is the strength of the valley-symmetry-breaking K-K' scattering. We show that the parametric variation in the level variance provides a quantitative measure for this scattering mechanism. We perform measurements of the parametric motion of Coulomb-blockade peaks as a function of magnetic field and find good agreement. We demonstrate that the magnetic-field dependence of graphene energy levels may serve as a sensitive indicator for the properties of graphene quantum dots and, in further consequence, for the validity of the Dirac picture.

DOI: 10.1103/PhysRevB.81.245411 PACS number(s): 73.22.Pr, 71.70.Di, 81.05.ue

I. INTRODUCTION

Graphene nanostructures[1–12] attract increasing attention mainly due to their potential applications in high mobility electronics[13,14] and solid-state quantum information processing.[15] In particular, low nuclear-spin concentrations expected in graphene promise long spin lifetimes[15–18] and make graphene quantum dots (QDs) (Refs. 1–4) interesting for spin-qubit operations.[15] Moreover, graphene nanostructures may allow to investigate phenomena related to massless Dirac Fermions in reduced dimensions.[1,19–25] Intensive research has been triggered by the unique electronic properties of graphene[26] including the gapless linear dispersion and the Landau-level (LL) spectrum.[27–35] Recent advances in fabricating width-modulated graphene nanoribbons have helped to overcome intrinsic difficulties in creating tunneling barriers and confining electrons in graphene, where transport is dominated by Klein tunneling-related phenomena.[36,37] Graphene QDs have been fabricated and Coulomb blockade,[1,2] quantum confinement,[3] and charge detection[4] have been demonstrated.

In this paper, we focus on the eigenenergies of graphene quantum dots (see Fig. 1) as a function of a perpendicular magnetic field. In graphene, the linear band crossing at the so-called Dirac point suggests a close connection between the dynamics of electrons and free, ultrarelativistic Dirac particles.[38] One might therefore expect a magnetic-field dependence of quantum dot eigenenergies that closely mirrors that of massless Dirac particles. Indeed, this connection has been used recently to discuss the spectrum of ideal, circular graphene dots with smooth confinement.[20,22] However, in more realistic models of finite graphene nanostructures, quantum confinement, edge effects, and lattice defects introduce a host of competing length scales absent from the simple Dirac picture. Much progress has been made in understanding the unique LL spectrum, and the resulting Hall effect, in graphene.[27–33] The magnetic-field dependence of the addition spectrum has been exploited in recent work to (approximately) pin down the electron-hole crossover point.[39] In the present paper we report on a systematic study of the B-field dependence of electronic eigenstates of graphene quantum dots of experimentally realizable size (diameter $d \leq 80$ nm). We highlight the interplay of different length scales controlling the breakdown of the valley symmetry by K-K' scattering. The latter is found to be key to the understanding of the diamagnetic spectrum. We find the B-field dependence of the level variance to be a sensitive measure for the strength of K-K' scattering and obtain good agreement with experimental Coulomb-blockade data.

The paper is organized as follows: we first briefly summarize the Dirac picture of Landau-level formation for massless charged Dirac particles and discuss the length scales relevant to its applicability to finite-size graphene quantum dots (Sec. II). In Sec. III we present realistic simulations for graphene quantum dots with zigzag and armchair edges, with edge roughness as well as with bulk disorder. A comparison between the calculated B-field dependence of the level variance and experimental data is given in Sec. IV, followed by a short summary (Sec. V).

II. DIRAC PICTURE AND ITS LIMITATIONS

The remarkable similarity of the low-energy band structure of graphene with the dispersion relation of a massless

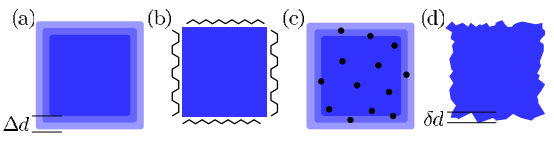

FIG. 1. (Color online) Shapes and sizes (50×50 nm^2) of graphene quantum dots confined by (a) a smooth valley spin-conserving potential [Eq. (11), the length scale of the confinement is marked by Δd], (b) atomically sharp armchair and zigzag boundaries. Dots with disorder due to (c) bulk defects or (d) edge roughness.

 ©2010 The American Physical Society

Dirac particle in two dimensions has been widely exploited in a variety of theoretical models for graphene.[26] However, the applicability of such models requires careful consideration of competing effects that go beyond the simple, yet intriguing Dirac picture.[40,41] A case in point is the diamagnetism, i.e., the magnetic response of a finite-size graphene quantum dot. It is of considerable interest to inquire into the applicability as well as the limitations of the well-known diamagnetic theory of charged massless Dirac fermions.

The magnetic-field (B) dependence of the spectrum of free Dirac particles was first solved in an early paper by Rabi[42] shortly after the Dirac equation was proposed. The Dirac equation for a massless particle with charge $q(=-|e|)$ in the presence of a potential $V(\mathbf{x})$ with timelike coupling and a perpendicular, homogeneous magnetic field $\mathbf{B}=\nabla\times\mathbf{A}=-By\nabla\times\mathbf{e_x}$ reads

$$H_D = H_0 + H_B = v_F\vec{\sigma}\cdot\left(\vec{p}-\frac{q}{c}\vec{A}\right)+\sigma_0 V(\vec{x}) \tag{1}$$

with $\vec{\sigma}=(\sigma_x,\sigma_y)$ the Pauli matrices and σ_0 the two-dimensional unit matrix. In the limiting case of strong magnetic field where $|qA/c|\gg|V(\mathbf{x})|$ the solution of Eq. (1) predicts the formation of Landau levels,[20–22,26,43]

$$E_n^D(B)=\mathrm{sgn}(n)\sqrt{2|e|\hbar v_F^2|n|B},\quad n\in\mathbb{Z}_0. \tag{2}$$

We explicitly label this reference spectrum with the superscript "D" (for Dirac equation). Equation (2) contains several remarkable features absent from nonrelativistic diamagnetism: a ground-state Landau level $n=0$ the energy of which does not depend on B at all. Higher Landau levels $n=\pm1,\pm2,\ldots$ are distributed symmetrically around $n=0$, and feature a $\sqrt{B}$ rather than a linear dependence on B known from nonrelativistic diamagnetism. The high-field regime [Eq. (2)] is controlled by just two length scales, the (energy-dependent) de Broglie wavelength λ_F and the magnetic length $l_B=\sqrt{\hbar c/(eB)}$. The strong (weak) field regime is characterized by $l_B\ll\lambda_F$ ($l_B\gg\lambda_F$). In the limit of weak magnetic fields, Eq. (1) predicts the lowest-order energy corrections to scale linearly with B, unlike the conventional nonrelativistic behavior ($\propto B^2$). Eigenstates of Eq. (1) form two-spinors with definite helicity (or "chirality")

$$\hat{h}|\psi\rangle=\frac{1}{2}\vec{\sigma}\cdot\frac{\vec{p}}{|p|}|\psi\rangle=\pm\frac{1}{2}|\psi\rangle \tag{3}$$

in the absence of external fields.

The ideal, infinitely extended graphene sheet featuring a honeycomb lattice made up by two interleafed triangular sublattices (A and B), can be described in nearest-neighbor tight-binding approximation by the Hamiltonian[44]

$$H=\sum_{i,s}|\phi_{i,s}\rangle V_i\langle\phi_{i,s}|-t\sum_{(i,j),s}|\phi_{i,s}\rangle\langle\phi_{j,s}|+\mathrm{H.c.}, \tag{4}$$

where the sum (i,j) extends over pairs of adjacent lattice sites, $|\phi_{j,s}\rangle$ is the tight-binding orbital at lattice site j, V_i is a locally varying potential, and t (on the order of 2.8 eV) is the nearest-neighbor hopping matrix element. [In the numerical calculations we take into account second- and third-nearest-neighbor coupling[24,45,46] in addition to Eq. (4) in order to quantitatively account for the realistic band structure.] Close to the Fermi energy, the band structure of Eq. (4) can be approximated (assuming that $V_i\ll t$) by a conical dispersion relation around the K point,[38]

$$E(k+k_K)=E(k_K)+k\partial_k E(k_K)+\mathcal{O}(k_K^2)\approx v_F|k|, \tag{5}$$

where we have set $E(k_K)=0$. Note that the above expansion ignores both the length scale of the graphene lattice constant $a=1.4$ Å and preferred directions of the lattice: due to the discrete lattice symmetry, the cone structure becomes squeezed along the K-K' directions, an effect known as triangular warping.[26,41] More importantly, the band structure features *two* nonequivalent cones (valleys) at the K and K' points in the reciprocal lattice. This additional degeneracy allows to formally represent the low-energy band structure near $E=0$ in terms of Dirac-type four-spinors $|\psi\rangle=(\psi_A^{(K)},\psi_B^{(K)},\psi_A^{(K')},\psi_B^{(K')})$ with amplitudes for the A-B sublattice in real space and for the K-K' valleys in reciprocal space. Operators in the four-spinor space can be represented by tensor products of $(\sigma_0,\vec{\sigma})$ matrices acting on A-B sublattice amplitudes and analogous $(\tau_0,\vec{\tau})$ Pauli matrices acting on K-K' amplitudes. Choosing the origin in k space such that the connecting line between K and K' is along y, the effective Dirac Hamiltonian in the absence of external scalar potentials becomes[47]

$$H_0=\vec{\sigma}\cdot\left(\vec{p}-\frac{q}{c}\vec{A}\right)\otimes\tau_1+\vec{\sigma}^*\cdot\left(\vec{p}-\frac{q}{c}\vec{A}\right)\otimes\tau_2, \tag{6}$$

where $\tau_{1,2}=(\tau_0\pm\tau_z)/2$. In addition to chirality, the valley-pseudospin projection

$$\tau_z|j\rangle=j|j\rangle,\quad j=\pm\frac{1}{2}, \tag{7}$$

associated with the valley degree of freedom is conserved. The upper ("particlelike," $E>0$) and lower ("holelike," $E<0$) cones touching each other at K and K' with $E=0$ are related to each other by a particle-hole transformation

$$\hat{C}=\sigma_z\otimes\tau_0,\quad \hat{C}H\hat{C}^{-1}=-H. \tag{8}$$

In the presence of a timelike scalar potential $V(\vec{x})\sigma_0\otimes\tau_0$, the Hamiltonian is invariant under an antiunitary transformation ("time reversal"), $\hat{T}=i\sigma_y\otimes\tau_0\mathcal{C}$, where $\mathcal{C}$ denotes complex conjugation.[26] The wave functions at K and K' are related by time-reversal symmetry. This symplectic symmetry ($T^2=-1$) is broken in the presence of a magnetic field

$$\hat{T}H(\vec{A})\hat{T}^{-1}=H(-\vec{A}), \tag{9}$$

lifting the twofold Kramers-type degeneracy. (Note that physical spin is not included in the present analysis.)

We now consider a finite-size system of linear dimension d, where $V(\mathbf{x})$ takes on the role of a confinement potential. With this additional length scale present, the Landau-level solution [Eq. (2)] is only valid in the strong magnetic-field regime with $l_B\ll d$ while in the weak-field regime, $l_B\gg d$, the spectrum will be determined by $V(\mathbf{x})$. For zero magnetic field, eigenstates $|\psi_K\rangle$ and $|\psi_{K'}\rangle$ localized at the K and K' points are degenerate. Turning on a magnetic field lifts this

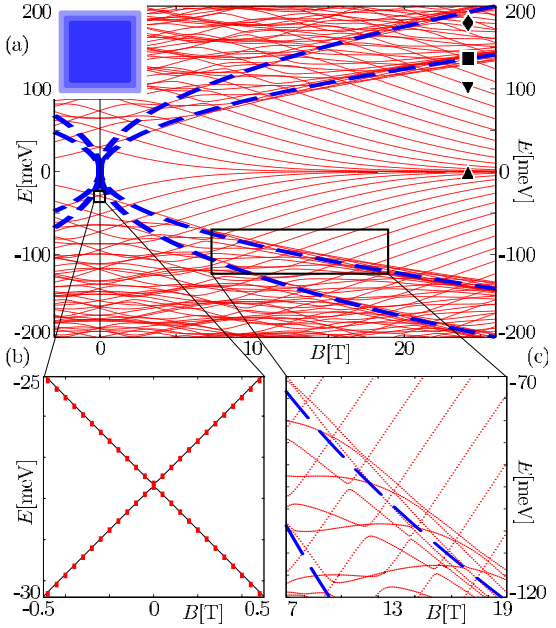

FIG. 2. (Color online) (a) Magnetic-field dependence of the eigenenergies of a graphene quantum dot with smooth confinement which approximately preserves valley symmetry [Eq. (11), see Fig. 1(a)]. Landau levels for $n=\pm 1, \pm 2$ [dashed lines, see Eq. (2)] are inserted as guide to the eye. The four symbols (▲, ▼, ■, and ♦) mark parameter values for which eigenstates are shown in Fig. 3. (b) Close-up of the avoided crossing of two eigenstates in (a). Dots represent numerical data, the continuous line is a fit to Eq. (10). (c) Closeup of avoided crossings around the diabatic ridge formed by the first Landau level (see text).

degeneracy without (to lowest order) introducing couplings between K and K'. Following first-order degenerate Rayleigh-Schrödinger perturbation theory, the perturbation matrix W describing the lowest-order correction to the field-free spectrum of Eq. (6) takes the form [for the gauge $A=(-By,0,0)$]

$$W = \langle H_B \rangle \sigma_x \otimes \tau_z, \tag{10}$$

where $\langle H_B \rangle_{KK} := Bq\langle \psi_B | y | \psi_A \rangle / c$ is real and linear in B. The perturbation preserves the valley symmetry. The absence of K-K' coupling and the linear magnetic-field dependence of $\langle H_B \rangle_{KK}$ for each decoupled Dirac cone implies that energy eigenvalues *linearly* cross the line $B=0$ in pairs of two, forming an X-shaped intersection (see Fig. 2). This is in contrast to the nonrelativistic diamagnetic response $\propto B^2$ in the perturbative limit. It rather resembles the paramagnetic level splitting in conventional quantum dots when the magnetic field lifts a degeneracy. Examples of the latter are lifting of Kramers' degeneracy[48] or a symmetry-induced degeneracy as in circular quantum dots.[49]

In order to quantitatively simulate the diamagnetic response of a finite-size graphene quantum dot we first consider a smooth confinement potential that is slowly varying on a length scale of the lattice constant such as to approximately conserve the valley-pseudospin projection τ_z (or valley symmetry). Moreover, it conserves particle-hole (anti)symmetry [Eq. (8)] in order to prevent Klein tunneling. Such a potential was first proposed by Berry and Mondragon[19] in the context of neutrino billiards,

$$V(\mathbf{x}) = V_0(e^{\Delta r(\mathbf{x})/\Delta d} - 1)\sigma_z, \tag{11}$$

where $\Delta r(\mathbf{x})$ is the outward distance from the quantum dot boundary and Δd introduces an additional length scale controlling the preservation of valley symmetry. We choose $\Delta d = 24$ Å [see Fig. 1(a)] much larger than the lattice spacing ($\Delta d \gg a \approx 1.42$ Å). Consequently, Eq. (11) varies slowly on the scale of the lattice constant, conserves valley symmetry [to order $(a/\Delta d)^2$], and provides a realization of the (approximately) K-K' decoupled diamagnetic perturbation [Eq. (10)]. We note that realizations of potentials of the form of Eq. (11) are, to our knowledge, currently experimentally not available. We employ a third-nearest-neighbor[40,45,46] tight-binding approximation (to correctly describe triangular warping) and simulate a 50×50 nm^2 graphene QD containing $\sim 100\ 000$ carbon atoms. The magnetic field is included by a Peierls phase factor. We use a Lanczos diagonalization in conjunction with an LU factorization to efficiently calculate the 500 eigenvalues closest to the Fermi edge[50,51] (see Fig. 2).

In the limit of weak magnetic fields, we find that our numerical results, indeed, follow the linear B-field dependence of the energy eigenvalues as predicted by perturbation theory [Eq. (10)] [see Fig. 2(b)]. Residual deviations from the perfect lattice symmetry (due to the finite width Δd of the confinement) and, thus, weak nonconservation of τ_z appear as minute energy splittings between near-degenerate levels in the $B \to 0$ limit. The resulting level splitting at $B=0$ is, however, very small (120 μeV), i.e., two orders of magnitude below the mean level spacing (~ 10 meV).

Turning now to the high-field limit, $l_B \ll d$, the influence of confinement effects should be diminished and the formation of Landau levels following the Dirac picture [Eq. (1)] is expected. The transition from low to high magnetic fields drastically changes the density of states (DOS). The depletion of the DOS near $E=0$ at low fields,

$$\rho(E) = \frac{d^2}{2(\hbar v_F)^2}|E|, \tag{12}$$

is replaced, for increasing B, by an increasing number of eigenstates moving toward the Landau level at E_0^D, which is located at the Dirac point [see Fig. 2(a)]. More specifically, all graphene levels with energies in between the two first Landau levels, $E_{-1}^D < E < E_1^D$, adiabatically converge to the level at $E_0^D = 0$. As we have shown recently,[39] this unique feature can be used to pin down the energetic position of the Dirac point in the experiment and thus of the electron-hole crossover region in real graphene quantum dot devices.

While, at low fields, the valley symmetry is approximately preserved by the potential in Eq. (11), a large number of sizeable avoided crossings appear at higher magnetic fields as the magnetic length is reduced to $l_B \ll d$. Edge states that couple to bulk states or to other edge states become prevalent. The complicated pattern in Figs. 2(a) and 2(c) of many avoided crossings near the first Landau energy $E=E_{\pm 1}^D$ reflects this interplay between magnetic bulk and

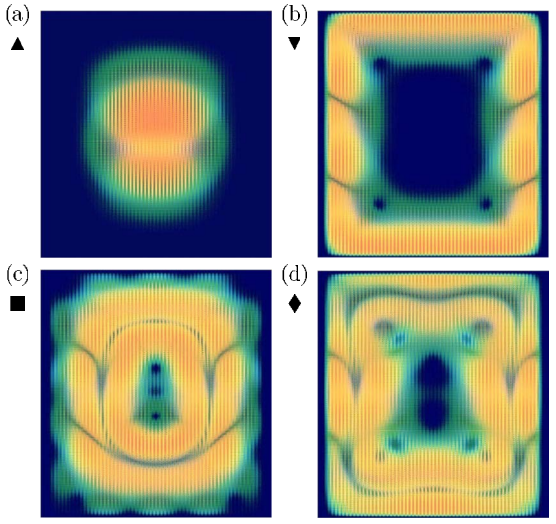

FIG. 3. (Color online) Typical eigenstates (plotted is the absolute square of the wave function) of a graphene quantum dot with smooth confinement [see Fig. 1(a) and Eq. (11)] at high magnetic field ($B=25$ T), corresponding to the zeroth [(a) and (b)] and first [(c) and (d)] Landau levels. Symbols (▲, ▼, ■, and ♦) correspond to those marking the position of these states in the energy level diagram [Fig. 2(a)].

edge states. Levels with eigenenergies that follow the predicted values for the Landau levels, E_n^D, are localized in the interior of the quantum dot and well separated from the edges. Conversely, the states with energies in between the values E_n^D should be strongly influenced by the spatial confinement in the quantum dot. Wave functions corresponding to energy levels close to $n=0$ and $n=1$ Landau levels [Figs. 3(a) and 3(c)] as well as those in between $n=0$ and $n=\pm 1$ [Fig. 3(b)] and between $n=1$ and $n=2$ [Fig. 3(d)] confirm these expectations.

Apparently, the typical level splittings at the avoided crossings [Figs. 2(b) and 2(c)] are dramatically enhanced in the high-field regime. This is due to the fact that, as compared to the low-field case, the amplitudes of wave functions are enhanced at the dot boundary [see Fig. 3(b)]. Since, in addition, the lattice symmetry is broken at the boundary, these edge states do have an increased coupling strength to all other states in the sample. Following the Wigner-von Neumann noncrossing rule[52] this increased coupling strength leads to increased level splittings at the crossing point.

III. REALISTIC GRAPHENE QUANTUM DOTS

A. Clean dots with sharp edges

We turn now to realistic graphene quantum dots where the nanostructures are terminated by atomically sharp edges, either of armchair or zigzag shape [Fig. 1(b)]. Following recent estimates for passivation of the dangling carbon bonds at the edges of graphene samples (e.g., by attached hydrogen),[53] we set the potential of the outmost carbon atoms to 1.7 eV. Although in this case many of the surface states present in a perfect zigzag boundary remain suppressed, such a confining potential leads to substantial

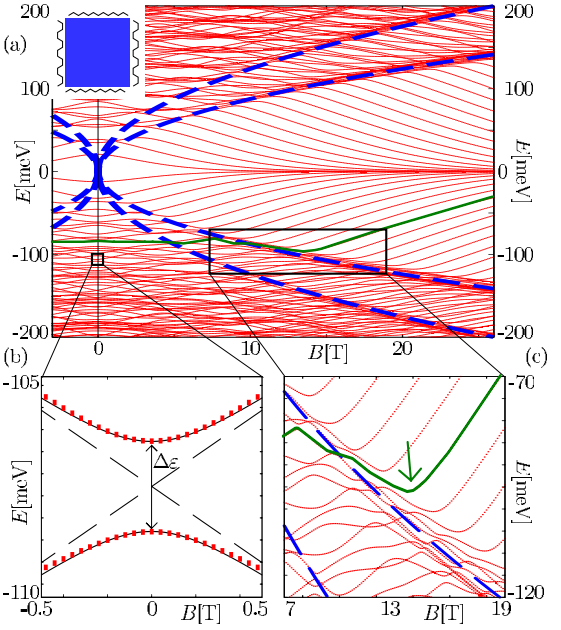

FIG. 4. (Color online) Same as Fig. 2 but for a quantum dot with atomically sharp zigzag and armchair boundaries. The solid line in (b) is a fit to Eq. (14), the dashed line (corresponding to $V_{KK'}=0$) is inserted as guide to the eye. The evolution of one eigenenergy with magnetic field is drawn with a thick solid line as guide to the eye in (a) and (c). The arrow in (c) marks a kink in the magnetic-field dependence of this state (see text).

changes in the energy-level spectrum [see Fig. 4(a)] as compared to the model potential [Eq. (11)]. Most importantly, in the low-field regime [see Fig. 4(b)] the linear B-field dependence is replaced by a quadratic dependence ($\propto B^2$) of the level splitting resembling the nonrelativistic diamagnetic response. This is due to the presence of sizable avoided crossings near $B=0$ as a result of broken valley symmetry caused by the edges. The valley symmetry is, thus, broken upon reflection at atomically sharp "clean" zigzag edges and τ_z is no longer conserved. In terms of perturbation theory, the confining potential V now includes off-diagonal components in the pseudospin degree of freedom

$$W = \sigma_x \otimes \langle H_B \rangle_{KK} \tau_z + \mathrm{Re}\langle V \rangle_{KK'} \tau_x + \mathrm{Im}\langle V \rangle_{KK'} \tau_y \quad (13)$$

with coupling matrix elements between the valleys $\langle V \rangle_{KK'} = \sigma_0 \otimes \langle \psi |_A V | \psi \rangle_{A'} + \sigma_x \otimes \langle \psi |_A V | \psi \rangle_{B'}$ and eigenvalues

$$\varepsilon = \pm \sqrt{\langle H_B \rangle_{KK}^2 + (\Delta\varepsilon/2)^2}, \quad \Delta\varepsilon = 2|\langle V_{KK'} \rangle|. \quad (14)$$

The coupling between K and K' cones thus leads, according to the Wigner-von Neumann noncrossing rule,[52] to avoided crossing with level splittings $\Delta\varepsilon$ [see Fig. 4(b)] proportional to the coupling strength $V_{KK'}$ between the two Dirac cones. Conversely, a fit to Eq. (14) yields a sensitive indicator for the amount of K-K' scattering in the quantum dot.

For high magnetic fields [see Fig. 4(c)], the presence of $V_{KK'}$ coupling lead to a large number of correlated avoided crossings when the edge states move toward the zeroth bulk Landau level. In other words avoided crossings appear when the energy of eigenstates evolving toward the E_0^D level "pass"

through the energy $E_1^D(B)$ of the first Landau level [Fig. 4(c)]. Due to a large number of avoided crossings, there are no states continuously following the first Landau level. We rather observe a bundle of states sequentially moving along the characteristic energy of the first Landau level, much like in a relay [see Fig. 4(c)]. Such an interrelated sequence of avoided crossings is well known from atomic physics as "diabatic ridge"—riding states localized on potential barriers.[54] A direct consequence is that the evolution of eigenstates for an increasing magnetic field [see highlighted line in Fig. 4(a)] features sharp "kinks" when crossing the ridge following the first Landau level [see arrow in Fig. 4(c)]. As the state is transiently trapped by the ridge, it moves away from the Dirac point and continues again monotonically toward the Dirac point once clear of the ridge. These kinks due to the ridge riding mechanism have been observed in the experiment[39] serving as an additional indicator for the position of the lowest Landau level and the electron-hole crossover.

The present results show that the atomically sharp edges destroy the linear B dependence of the energy levels at weak fields but they do preserve the square-root B dependence at very high fields. The linear B dependence results from the fragile suppression of K-K' scattering ($\propto\langle V\rangle_{KK'}$) between the Dirac cones while the square-root dependence results from the much more robust dispersion relation of the individual cone. Therefore, Landau levels survive the introduction of sharp boundaries much better than the energy levels at weak fields. In turn, even when in the experiment a Dirac-type Landau-level spectrum is recorded, many other features of the same graphene sample may very well show large deviations from predictions based on Dirac theory.

B. Dots with bulk disorder

To further elucidate the role of lattice symmetry breaking in graphene quantum dots, we now consider isolated lattice defects in the bulk. The preceding results suggest that disorder realizations that break the K-K' symmetry are of crucial importance. We therefore consider first single-lattice vacancies [see inset in Fig. 5(a)] with defect densities of $n_i = 10^{-5} - 10^{-3}$ impurities per carbon atom. To isolate the effect of such bulk defects from the K-K' scattering of the edges, we first use the smooth symmetry preserving boundary potential [see Eq. (11)]. Overall, the diamagnetic spectrum closely resembles that of clean samples with atomically sharp edges (see Fig. 5). In particular, avoided crossings near $B=0$ with a quadratic field dependence as well as the formation of sequences of avoided crossings along the ridges of bulk Landau levels are found. Wave functions of eigenstates at these energies display patterns which are very similar to those for the clean system [compare Figs. 3(b) and 6(a)]. Likewise, the kink pattern at the crossing of the ridges appears robust against disorder [see, e.g., Fig. 5(c)]. We do, however, observe new ridges between the Landau-level energies which were absent for edge scattering [see dotted lines in Figs. 5(a) and 5(c)]. The corresponding eigenstates near these new ridges [see Fig. 6(b), marked by ▼ in Fig. 5(a)] are pinned to a single defect, where the lattice periodicity

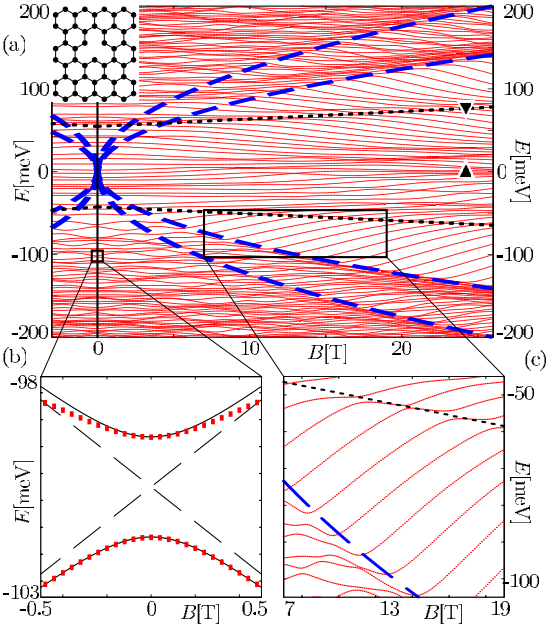

FIG. 5. (Color online) Same as Fig. 2 for a quantum dot featuring 30 single-lattice vacancies (see inset) out of a total number of 100.000 carbon atoms. Dotted lines mark the evolution of two states localized at one defect. Symbols mark the states for which the corresponding wave function is shown in Fig. 6.

and the A-B sublattice symmetry are broken, and the partitioning of the wave function in four components according to the Hamiltonian in Eq. (6) fails. Such localized states can therefore be expected to behave differently from the bulk Landau levels. The resulting ridges feature a very weak quasilinear magnetic-field dependence. We therefore conjecture that these structures are due to avoided crossings with such localized defect states. Recent analysis[55,56] has shown that K-K' scattering at impurities in graphene, i.e., the strength of

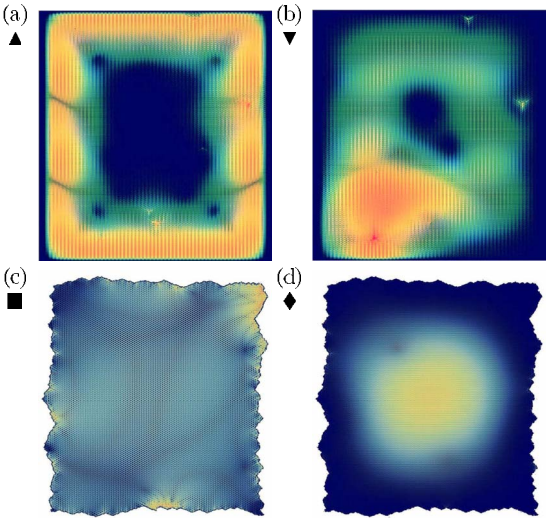

FIG. 6. (Color online) Eigenstates of a graphene quantum dot with disorder: (▲ and ▼) 30 single vacancies [one single vacancy shown as inset in Fig. 5(a)] or (■ and ♦) edge roughness of ±2 nm. Positions in the energy level diagram are marked by corresponding symbols in Figs. 5(a) and 8(a).

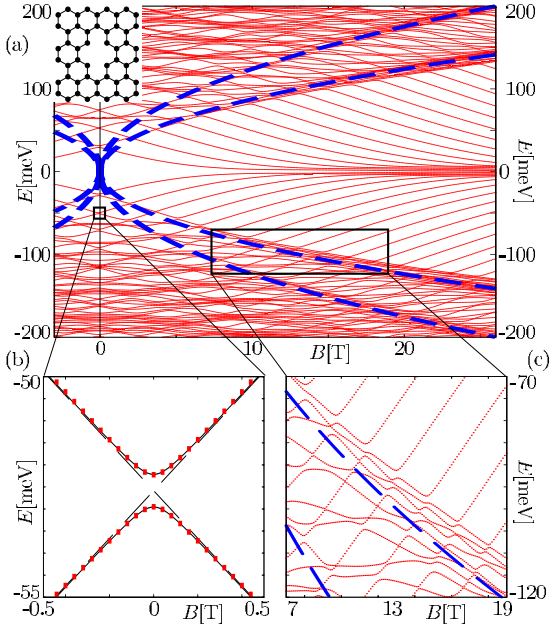

FIG. 7. (Color online) Same as Fig. 2 for a quantum dot featuring 30 double lattice vacancies (see inset) in 100.000 carbon atoms.

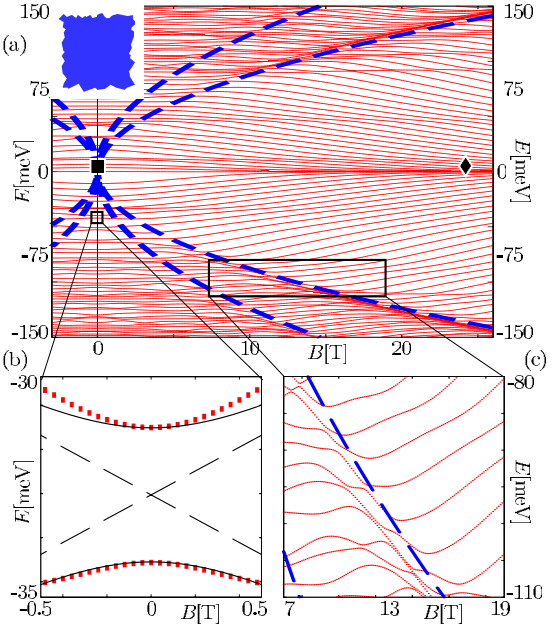

FIG. 8. (Color online) Same as Fig. 4 for a quantum dot featuring rough edges (with a roughness amplitude $\delta d = \pm 2$ nm). Symbols mark the states for which the corresponding wave function is shown in Fig. 6.

$V_{KK'}$, tends to be strongly energy dependent. Bound states due to adsorbates (leading to an enhanced local density of states at the adsorption site) frequently have energies close to the Dirac point.[56,57] Since the localized defect states with energy E_n feature a very weak explicit linear magnetic-field dependence,

$$E_n[V_{KK'},B] \approx E_n[V_{KK'}] + \alpha|B|, \quad |\alpha| < 1 \ \text{meV/T}, \tag{15}$$

the implicit magnetic-field dependence of $V_{KK'}(E_n[B])$ may be neglected. While the detailed energy dependence of $V_{KK'}$ may be connected to the specific defect present (e.g., Stone-Wales defects or attached nitrogen molecules), we still qualitatively expect an analogous linear B-field dependence. Such localized states with weak magnetic-field dependence were also observed experimentally in Coulomb-blockade measurements.[39,58]

In the low-field regime, we observe a significant change in the B evolution of eigenenergies: avoided crossings become asymmetric [see Fig. 5(b)]. The reason is that the K-K' splitting introduced by the lattice vacancies is strong enough to yield different matrix elements for $\langle H\rangle_{KK}$ and $\langle H\rangle_{K'K'}$: consequently, the slope of both eigenvalues of Eq. (13) is different [see Fig. 5(b)]. To illustrate that the diamagnetic spectrum, in particular the avoided crossing distribution, is due to the breaking of the A-B sublattice and, in turn, to the breaking of valley pseudospin symmetry induced by the defects, we present as counter example the spectrum for double vacancies. We introduce such a vacancy in accordance to our soft-wall potential, Eq. (11). As such double vacancies act on an entire unit cell in the hexagonal lattice, they approximately conserve the electron-hole and K-K' symmetry. We find, indeed, that for the same number of defects as of single vacancies (Fig. 5), only avoided crossings with comparatively small energy splittings appear in the energy-level diagram (Fig. 7), resembling much more closely Fig. 3. This clearly indicates that it is the breaking of the A-B symmetry and not the presence of defects *per se* which is responsible for the breakdown of the Dirac picture for graphene quantum dots.

C. Dots with edge disorder

We consider now a clean graphene quantum dot with atomically sharp but disordered edges. We connect short straight edge segments (with a random length between 0.5 and 3 nm) to obtain a polygon-shaped boundary [see Fig. 1(c)] with a disorder amplitude of $|\delta d| \leq 2$ nm. δd is thus (at energies close to the Dirac point) smaller than the wavelength λ_F of the confined particles as well as the magnetic length but larger than the lattice constant. Since rough boundaries, just like bulk defects, localize states,[23,24] we expect similar signatures of these two types of disorder. Indeed, in the low-field regime, dots with rough edges feature a similar pattern of fluctuating energy levels as dots with single-lattice defects (compare Figs. 5 and 8). The spectra are so similar that it is difficult to distinguish between bulk and edge disorder breaking the K-K' symmetry. Also in the high-field regime, the evolution toward the Landau levels features the correlated sequence of avoided crossings reflecting the diabatic ridges [see Fig. 8(c)]. Wave functions of eigenstates at these energies display patterns which are very similar to those for the clean system [compare Figs. 3(a) and 6(d)]. In particular, states near Landau levels localize in the interior of the dot and thus are not influenced by edge disorder. Likewise, the kink pattern at the crossing of the ridges is robust against edge disorder. While the inclusion of edge disorder

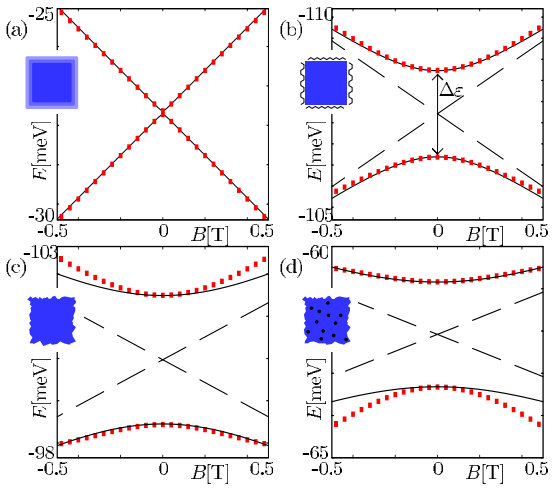

FIG. 9. (Color online) (Avoided) crossings for (a) soft edges, (b) hard edges, (c) rough edges, and (d) rough edges plus bulk disorder. The level splitting is (a) 0.1 meV, (b) 2 meV, (c) 3 meV, and (d) 2.5 meV.

does not give rise to qualitatively new effects on the eigenenergy spectrum in the high-field regime, differentiating between edge and bulk disorder might become possible by probing the different scaling behavior for bulk and edge disorder with the size of the graphene quantum dot.

It is instructive to directly contrast the level splitting $\Delta\varepsilon$ of an avoided crossing [Eq. (14)] due to finite K-K' coupling for different scenarios: (i) valley-symmetry preserving confinement [Fig. 9(a)], (ii) clean graphene quantum dots with atomically sharp edges [Fig. 9(b)], and (iii) disordered graphene quantum dots [Figs. 9(c) and 9(d)]. We observe an increase in the size of the average level splitting $\langle\Delta\varepsilon\rangle$ due to K-K' coupling at the edges and impurities. In scenario (i) $\langle\Delta\varepsilon\rangle$ is at least one order of magnitude smaller than the mean level spacing $\langle\delta\varepsilon\rangle$, $\langle\Delta\varepsilon\rangle \ll \langle\delta\varepsilon\rangle$. In (ii) where $\langle\Delta\varepsilon\rangle < \langle\delta\varepsilon\rangle$ a first-order perturbative treatment of K-K' coupling correctly describes the level repulsion. For localization at defects (iii) where $\langle\Delta\varepsilon\rangle \lesssim \langle\delta\varepsilon\rangle$ level pairs at K and K' feature different quadratic dependences on B, and can no longer be parametrized by Eqs. (13) and (14).

IV. COMPARISON WITH EXPERIMENT: LEVEL SPACING FLUCTUATIONS

For a comparison with the experimental data for the magnetic response of graphene quantum dots we pursue two strategies: in a direct approach we compare our models with the observed parametric B-field evolution of individual Coulomb-blockade peaks. Alternatively, we identify the B-field dependence of the level spacing fluctuations (variance) as a robust measure for the degree of disorder in a graphene quantum dot. Specifically, we determine the rescaled (or unfolded) variance σ_ε of the distribution of neighboring energy-level spacings $\delta\varepsilon$

$$\sigma_\varepsilon := \frac{1}{\langle\delta\varepsilon\rangle}\sqrt{\langle(\delta\varepsilon)^2 - \langle\delta\varepsilon\rangle^2\rangle}. \tag{16}$$

Since switching on a magnetic field B leaves the number of states unchanged, $\langle\delta\varepsilon\rangle$ is (approximately) independent of B,

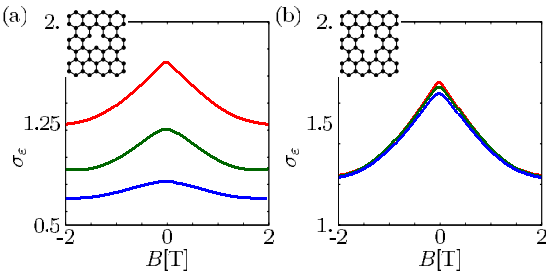

FIG. 10. (Color online) Variance σ_ε of the mean level spacing [see Eq. (16)] as a function of magnetic field for (a) single-vacancy defects and (b) double-vacancy defects (note the expanded y scale) for three values of disorder concentrations: from top to bottom $n_i = 3\times10^{-5}$, 6×10^{-5}, and 2×10^{-4}.

while higher moments of the level distribution are drastically affected. At $B=0$, pairs of energy levels are split by the characteristic energy $\Delta\varepsilon$ of the avoided level crossings. However, as long as the mean width of the avoided crossing $\langle\Delta\varepsilon\rangle$ [Eq. (14)] is small compared to the mean level spacing $\langle\delta\varepsilon\rangle$, the level sequence fluctuates between small and large spacings while spacings on the order of $\delta\varepsilon$ are unlikely. We thus expect for magnetic field $B=0$ a comparatively large variance σ_ε. For increasing $|B|$ the levels become more equi-spaced, leading to a decrease in σ_ε. Correspondingly, the variance σ_ε of the level spacings should feature a peak at $B=0$. The numerical results for the dependence of σ_ε on B for different disorder strength (i.e., different $|V_{KK'}|$) are shown in Fig. 10. Our data display a pronounced peak of σ_ε for the clean flake slowly decreasing for increasing number of single-vacancy defects (i.e., for increasing K-K' scattering) [see Fig. 10(a)]. Note that both the peak height at $B=0$ and the overall value of σ_ε decrease with increasing disorder. The latter can be explained by the emerging localized states that feature a regular spacing (and hence a suppressed variance σ_ε). Consequently, if a given spectral region is more prone to feature localized states due to adsorbates than others,[56,57] we expect an energy dependence on σ depending on the specific type of adsorbate. Such an energy dependence could be exploited to directly measure the energy dependence of K-K' scattering by determining the statistics of Coulomb-blockade resonances at different back-gate voltages. For comparison we also show σ_ε for double vacancies preserving A-B symmetry. [See Fig. 10(b), note the different scales.] Accordingly, σ_ε is, indeed, strongly dependent on the amount of K-K' scatterers, not on the overall number of defects.

The decrease in peak height with increasing K-K' scattering should thus provide a robust and sensitive measure for K-K' scattering present in the experiment. To test this conjecture, we have measured the evolution of 42 Coulomb-blockade peaks for varying magnetic field.[59] We follow the parametric motion of the peak positions, and hence the eigenstate energies, as a function of magnetic field $B \in [-2,2]$ T. To compare with our numerical results, we take into account a charging energy of 13 meV (determined independently[59]) as well as spin (by Zeeman splitting). We observe, indeed, a quadratic B-field dependence rather than the linear dependence predicted for conserved K-K' symmetry of the Dirac equation. Our experimental data can be well

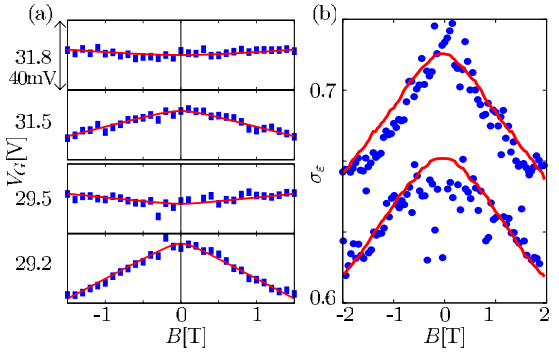

FIG. 11. (Color online) (a) Coulomb-blockade peaks measured as a function of applied plunger gate electrode potential (V_G) and magnetic field applied perpendicular to the sample (see Ref. 59 for details about the measurement). Lines: fit to Eq. (14) for two measured Coulomb-blockade peak pairs with a level splitting at $B=0$ of ≈ 0.3 V. (b) Normalized variance of the level spacing σ_ε [see Eq. (16)] as a function of magnetic field. Dots denote an average over 20 consecutive experimental Coulomb-blockade peaks for two values of back-gate voltage V_{BG} [corresponding to the upper ($V_{BG}=20$ V) and lower ($V_{BG}=38$ V) data points]. Solid lines represent simulations for different edge roughness amplitude δd [Fig. 1(d)] as only fit parameter: $\delta d \approx 0.5$ (0.6) nm, for the upper (lower) curve.

described by Eq. (14) [see Fig. 11(a)]. For pairs of consecutive Coulomb-blockade resonances belonging to the same avoided crossing, we find a mismatch in slopes, in agreement with our numerical findings for the rough-edged quantum dot [compare Figs. 9(c), 9(d), and 11(a)]. This has important consequences for the interpretation of experimental data: the roughness present in the experimental dot does not allow to disentangle K and K' states. To be more quantitative, we compare our simulations for the level variance with experimental data. We indeed find good agreement as confirmed by a noticeable peak also in the experimental data for $\sigma_\varepsilon(B)$ [see Fig. 11(b)]. The offset between the two data sets in Fig. 11(b) is attributed to a possible energy dependence of K-K' scattering as well as statistical fluctuations in charging energy and in the number of localized states for different values of the back-gate voltage. By using the edge roughness δd as the only adjustable parameter, we can match the measured $\sigma_\varepsilon(B)$ very well with our numerical simulation [see lines in Fig. 11(b)]. Good agreement is found for an edge roughness of about $\delta d \approx 0.5 \pm 0.2$ nm, or, equivalently, a K-K' scatterer concentration in the bulk $n_i \approx (3.5 \pm 1) \times 10^{-4}$, both of which are well within expectation. We emphasize that, although we can quantify the resulting overall strength of K-K' coupling in our experimental quantum dot, we cannot disentangle whether the observed K-K' scattering comes from edge roughness, lattice defects, or disorder through flake-substrate interactions with a length scale comparable to the lattice constant.

V. CONCLUSIONS

We have investigated the evolution of eigenstates in graphene quantum dots with increasing magnetic field. Concentrating on the energy regime around the Dirac point, we observe a smooth transition from a linear density of states to the emergence of Landau levels. At high-field strength, we find that Landau levels follow the square-root dependence of the Dirac equation, manifested in the energy-level diagram by sequences of correlated avoided crossings along diabatic ridges. These ridges lead to characteristic kinks in the evolution of energy states that cross a Landau level. Appearing also in Coulomb-blockade measurements, these kinks can be used to experimentally pin down the electron-hole crossover point.[39] In the perturbative regime of small magnetic fields, we find that the linear dependence on B predicted by the model of massless Dirac fermions disappears when the valley symmetry is broken. Even perfect armchair and zigzag edges are sufficient to break the sublattice symmetry giving rise to avoided crossings with a quadratic dependence on B instead. A similar effect is observed for lattice defects: single-lattice vacancies break the K-K' symmetry and thus result in avoided crossings with substantial level splittings (even for defect concentrations as low as 1 in 20.000). By comparison with double vacancies which conserve the sublattice symmetry we show that it is not the presence of disorder *per se* which leads to deviations from predictions by the Dirac equation but the breaking of valley symmetry.

We compare our theoretical predictions with experimental results on the parametric B-field evolution of Coulomb-blockade peaks. As a quantitative indicator for the strength of K-K' scattering, we identify the variance σ_ε of the level spacing distribution. We observe a peak in the variance at $B=0$ due to level correlations near avoided crossings. We find quantitative agreement between the measured and the calculated data for σ_ε which enables us to pinpoint the amount of K-K' scattering present in our experimental flake. The present results provide a sensitive indicator for the quality of the graphene dot and demonstrate the limits of the Dirac picture in describing the experiment.

ACKNOWLEDGMENTS

We thank K. Ensslin, T. Ihn, and M. Wimmer for valuable discussions. F.L. and J.B. acknowledge support from the FWF under Grants No. SFB 016 and No. SFB 041, J.G. from the Swiss National Science Foundation, and C.S. support from NCCR. Computational resources from the Vienna Scientific Cluster (VSC) are gratefully acknowledged.

*Corresponding author; florian@concord.itp.tuwien.ac.at

[1] L. A. Ponomarenko, F. Schedin, M. I. Katsnelson, R. Yang, E. H. Hill, K. S. Novoselov, and A. K. Geim, Science **320**, 356 (2008).

[2] C. Stampfer, J. Güttinger, F. Molitor, D. Graf, T. Ihn, and K. Ensslin, Appl. Phys. Lett. **92**, 012102 (2008); C. Stampfer, E. Schurtenberger, F. Molitor, J. Güttinger, T. Ihn, and K. Ensslin, Nano Lett. **8**, 2378 (2008).

[3] S. Schnez, F. Molitor, C. Stampfer, J. Güttinger, I. Shorubalko, T. Ihn, and K. Ensslin, Appl. Phys. Lett. **94**, 012107 (2009).

[4] J. Güttinger, C. Stampfer, S. Hellmüller, F. Molitor, T. Ihn, and K. Ensslin, Appl. Phys. Lett. **93**, 212102 (2008).

[5] M. Y. Han, B. Özyilmaz, Y. Zhang, and P. Kim, Phys. Rev. Lett. **98**, 206805 (2007).

[6] Z. Chen, Y.-M. Lin, M. J. Rooks, and P. Avouris, Physica E (Amsterdam) **40**, 228 (2007).

[7] X. Li, X. Wang, L. Zhang, S. Lee, and H. Dai, Science **319**, 1229 (2008).

[8] K. Todd, H.-T. Chou, S. Amasha, and D. Goldhaber-Gordon, Nano Lett. **9**, 416 (2009).

[9] X. Liu, J. B. Oostinga, A. F. Morpurgo, and L. M. K. Vandersypen, Phys. Rev. B **80**, 121407(R) (2009).

[10] J. Moser and A. Bachtold, Appl. Phys. Lett. **95**, 173506 (2009).

[11] C. Stampfer, J. Güttinger, S. Hellmüller, F. Molitor, K. Ensslin, and T. Ihn, Phys. Rev. Lett. **102**, 056403 (2009).

[12] K. A. Ritter and J. W. Lyding, Nature Mater. **8**, 235 (2009).

[13] A. K. Geim and K. S. Novoselov, Nature Mater. **6**, 183 (2007).

[14] M. I. Katsnelson, Mater. Today **10**, 20 (2007).

[15] B. Trauzettel, D. V. Bulaev, D. Loss, and G. Burkard, Nat. Phys. **3**, 192 (2007).

[16] C. L. Kane and E. J. Mele, Phys. Rev. Lett. **95**, 226801 (2005).

[17] H. Min, J. E. Hill, N. A. Sinitsyn, B. R. Sahu, L. Kleinman, and A. H. MacDonald, Phys. Rev. B **74**, 165310 (2006).

[18] D. Huertas-Hernando, F. Guinea, and A. Brataas, Phys. Rev. B **74**, 155426 (2006).

[19] M. V. Berry and R. J. Mondragon, Proc. R. Soc. London, Ser. A **412**, 53 (1987).

[20] S. Schnez, K. Ensslin, M. Sigrist, and T. Ihn, Phys. Rev. B **78**, 195427 (2008).

[21] P. Recher, B. Trauzettel, A. Rycerz, Ya. M. Blanter, C. W. J. Beenakker, and A. F. Morpurgo, Phys. Rev. B **76**, 235404 (2007).

[22] P. Recher, J. Nilsson, G. Burkard, and B. Trauzettel, Phys. Rev. B **79**, 085407 (2009).

[23] M. Wimmer, A. R. Akhmerov, and F. Guinea, arXiv:1003.4602 (unpublished).

[24] F. Libisch, C. Stampfer, and J. Burgdörfer, Phys. Rev. B **79**, 115423 (2009).

[25] A. F. Young and P. Kim, Nat. Phys. **5**, 222 (2009).

[26] For review see, e.g., A. H. Castro Neto, F. Guinea, N. M. R. Peres, K. S. Novoselov, and A. K. Geim, Rev. Mod. Phys. **81**, 109 (2009).

[27] F. D. M. Haldane, Phys. Rev. Lett. **61**, 2015 (1988).

[28] Y. Zheng and T. Ando, Phys. Rev. B **65**, 245420 (2002).

[29] E. McCann and V. I. Fal'ko, Phys. Rev. Lett. **96**, 086805 (2006).

[30] L. Sheng, D. N. Sheng, F. D. M. Haldane, and L. Balents, Phys. Rev. Lett. **99**, 196802 (2007).

[31] P. M. Ostrovsky, I. V. Gornyi, and A. D. Mirlin, Phys. Rev. B **77**, 195430 (2008).

[32] D. A. Bahamon, A. L. C. Pereira, and P. A. Schulz, Phys. Rev. B **79**, 125414 (2009).

[33] P. H. Rivera, A. L. C. Pereira, and P. A. Schulz, Phys. Rev. B **79**, 205406 (2009).

[34] K. S. Novoselov, A. K. Geim, S. V. Morozov, D. Jiang, M. I. Katsnelson, I. V. Grigorieva, S. V. Dubonos, and A. A. Firsov, Nature (London) **438**, 197 (2005).

[35] Y. Zhang, Y.-W. Tan, H. L. Stormer, and P. Kim, Nature (London) **438**, 201 (2005).

[36] N. Dombay and A. Calogeracos, Phys. Rep. **315**, 4158 (1999).

[37] M. I. Katsnelson, K. S. Novoselov, and A. K. Geim, Nat. Phys. **2**, 620 (2006).

[38] G. W. Semenoff, Phys. Rev. Lett. **53**, 2449 (1984).

[39] J. Güttinger, C. Stampfer, F. Libisch, T. Frey, J. Burgdörfer, T. Ihn, and K. Ensslin, Phys. Rev. Lett. **103**, 046810 (2009).

[40] K. Sasaki, S. Murakami, and R. Saito, Appl. Phys. Lett. **88**, 113110 (2006).

[41] E. McCann, K. Kechedzhi, V. I. Fal'ko, H. Suzuura, T. Ando, and B. L. Altshuler, Phys. Rev. Lett. **97**, 146805 (2006).

[42] I. I. Rabi, Zeitschrift f. Physik A **49**, 507 (1928).

[43] J. W. McClure, Phys. Rev. **104**, 666 (1956).

[44] P. R. Wallace, Phys. Rev. **71**, 622 (1947).

[45] S. Reich, J. Maultzsch, C. Thomsen, and P. Ordejón, Phys. Rev. B **66**, 035412 (2002).

[46] A. Grüneis, C. Attaccalite, L. Wirtz, H. Shiozawa, R. Saito, T. Pichler, and A. Rubio, Phys. Rev. B **78**, 205425 (2008).

[47] J. C. Slonczewski and P. R. Weiss, Phys. Rev. **109**, 272 (1958).

[48] S. Adam, M. L. Polianski, X. Waintal, and P. W. Brouwer, Phys. Rev. B **66**, 195412 (2002).

[49] C. S. Lent, Phys. Rev. B **43**, 4179 (1991).

[50] C. Lanczos, J. Res. Natl. Bur. Stand. **45**, 255 (1950).

[51] P. R. Amestoy, I. S. Duff, J. Koster, and J.-Y. L'Excellent, SIAM J. Matrix Anal. Appl. **23**, 15 (2001); P. R. Amestoy, A. Guermouche, J.-Y. L'Excellent, and S. Pralet, Parallel Comput. **32**, 136 (2006).

[52] J. von Neumann and E. P. Wigner, Z. Phys. **30**, 467 (1929).

[53] Y.-W. Son, M. L. Cohen, and S. G. Louie, Phys. Rev. Lett. **97**, 216803 (2006).

[54] P. S. Krstić, C. O. Reinhold, and J. Burgdörfer, Phys. Rev. A **63**, 052702 (2001); see also J. Burgdörfer, N. Rohringer, P. S. Krstić, and C. O. Reinhold, in *Nonadiabatic Transition in Quantum Systems*, edited by V. I. Osherov and L. I. Ponomarev (Institute of Chemical Physics, RAS, Chernogolovka, Russia, 2004), p. 205.

[55] Yu. V. Skrypnyk and V. M. Loktev, Phys. Rev. B **73**, 241402(R) (2006).

[56] J. P. Robinson, H. Schomerus, L. Oroszlány, and V. I. Fal'ko, Phys. Rev. Lett. **101**, 196803 (2008).

[57] T. O. Wehling, M. I. Katsnelson, and A. I. Lichtenstein, Phys. Rev. B **80**, 085428 (2009).

[58] J. Güttinger, C. Stampfer, T. Frey, T. Ihn, and K. Ensslin, Phys. Status Solidi B **246**, 2553 (2009).

[59] The measured graphene quantum dot had a similar geometry as the dot described in Refs. 39 and 58. By changing the potential of the back-gate electrode (V_G) a region of suppressed current between $V_G=10$ and 45 V was found. From measurements of Coulomb-blockade peaks in this region (with $\approx$150 Coulomb peaks) a charging energy of $\approx$13 meV was extracted. For more details about the measurements see Refs. 39 and 58.